

Properties of helium defects in bcc and fcc metals investigated with density functional theoryX. T. Zu,^{1,*} L. Yang,¹ F. Gao,^{2,†} S. M. Peng,³ H. L. Heinisch,² X. G. Long,³ and R. J. Kurtz²¹*Department of Applied Physics, University of Electronic Science and Technology of China, Chengdu 610054, People's Republic of China*²*Pacific Northwest National Laboratory, P.O. Box 999, Richland, Washington 99352, USA*³*Institute of Nuclear Physics and Chemistry, China Academy of Engineering Physics, Mianyang 621900, People's Republic of China*

(Received 25 March 2009; published 12 August 2009)

The relative stability of single He defects in bcc and fcc metals is investigated using *ab initio* calculations based on density functional theory. The results indicate that the tetrahedral position is energetically more favorable for a He interstitial than the octahedral site in bcc metals, but the relative stability of He defects in fcc metals varies, depending on local environments. The He formation energies in bcc Fe and fcc Ni at the tetrahedral and octahedral positions with and without spin polarization are investigated. It is of interest to find that the magnetism of host atoms does not directly affect the relative stabilities of He in interstitial sites in bcc Fe and fcc Ni.

DOI: [10.1103/PhysRevB.80.054104](https://doi.org/10.1103/PhysRevB.80.054104)

PACS number(s): 31.15.es, 61.72.J-, 61.80.-x, 74.62.Dh

I. INTRODUCTION

The interaction of a helium impurity with a metal is of fundamental importance within a fusion reactor environment, where the first wall will be exposed to a high flux of helium escaping from the plasma.¹ Because of the extremely low solubility of helium in materials, helium atoms tend to be trapped at defects that contain regions of excess volume, such as vacancies, dislocations, and grain boundaries, and they consequently form helium bubbles (or voids).²⁻⁵ The formation of helium bubbles in materials can lead to void swelling and produces high temperature intergranular embrittlement, surface roughening, and blistering,⁶ which can significantly degrade the mechanical properties of materials.

It is impossible to directly obtain experimentally the detailed configurations and relative stabilities of He atoms in various metals at the scale needed for understanding He behavior. However, theoretical and modeling methods can provide valuable understanding. In earlier investigations⁷ a calculation scheme which combines a pair-potential approach with the effective-medium theory was used to evaluate interstitial He formation energies, finding that in bcc metals (K, Fe, Mo, and W), their formation energies are nearly equal at the tetrahedral and octahedral interstitial positions. In the fcc metal Ni, the octahedral site was found to be a favorable position for interstitial helium. Recently, first-principles methods have been employed to study the physical properties of He defects in bcc iron,⁸ and the calculated results reveal that the tetrahedral position is energetically more favorable for a He interstitial than the octahedral site due to the influences of the magnetic interactions.

In the present paper, the relative stabilities of single He defects in several bcc and fcc metals are investigated with *ab initio* calculations based on density functional theory (DFT), using the Vienna *ab initio* simulation package (VASP).⁹⁻¹¹ The interstitial He formation energies at the tetrahedral and octahedral positions are calculated using *ab initio* method. Furthermore, the electronic density of states (DOS) and charge density difference of He atom and its first neighbor Fe are analyzed to address the effects of magnetism on the relative stabilities of He defects in bcc Fe.

II. METHODOLOGY

The present calculations have been performed within DFT as implemented in the VASP.⁹⁻¹¹ The interaction between ions and electrons is described by the projector-augmented wave (PAW) method^{12,13} for different metals. Exchange and correlation functions were taken in a form proposed by Perdew and Wang (PW91)¹⁴ within the generalized gradient approximation (GGA). The supercell approach with periodic boundary conditions was used to study defect properties, as well as pure metal systems. The supercells contain 128 and 108 atoms for bcc and fcc metals, respectively. The effects of the supercell size on the results have been investigated for bcc metals. The relaxations of the atomic position and optimizations of the shape and size of the supercells were performed with the plane-wave basis sets with the energy cutoff of 500 eV throughout this work. Ion relaxations were performed using the standard conjugated-gradient algorithms as implemented in the VASP code. During the relaxations, the Brillouin zone (BZ) integration was achieved using a Methfessel-Pazton smearing of $\sigma=0.2$ eV. BZ sampling was performed using the Monkhorst-Pack scheme, with $5 \times 5 \times 5$ k -point meshes for a 56 atom supercell and $3 \times 3 \times 3$ k -point meshes for a 128 atom supercell in bcc metals and $3 \times 3 \times 3$ k -point meshes for a 108 atom supercell in fcc metals. We have tested these k -point meshes for different metals considered, which give converged results in terms of defect formation energy.

The ground-state properties of bcc and fcc metals, including equilibrium lattice parameters (a_0), cohesive energies (E_{coh}), and vacancy formation energy (E_v^f) have been calculated to evaluate the pseudopotentials used in the present work. The fully relaxed results are summarized in Table I along with the experimental values for comparison. It can be seen from Table I that the calculations are in good agreement with the available experimental values, which suggest that the chosen pseudopotentials are appropriate to describe the structural properties of the relevant metals. In addition, the PAW pseudopotential was used to describe the He properties, whereas exchange and correlation functions were taken in PW91 within the GGA. The defect formation energy is defined as

TABLE I. Ground-state properties of bcc and fcc metals, including equilibrium lattice parameters (a_0), cohesive energies (E_{coh}), and vacancy formation energies (E_v^f). The calculations were done using 128 and 108 atom supercells for bcc metals and fcc metals with 27 k points, respectively.

		bcc				fcc			
		Fe	Cr	Mo	W	Ni	Cu	Ag	Pd
		PAW, PW91	PAW, PW91	PAW, PW91	PAW, PW91	PAW, PW91	PAW, PW91	PAW, PW91	PAW, PW91
a (Å)	Pres.	2.829	2.836	3.154	3.175	3.519	3.634	4.153	3.859
	Expt. ^a	2.865	2.910	3.147	3.162	3.524	3.615	4.085	3.962
E_{coh} (eV)	Pres.	5.26	4.03	10.62	6.90	4.84	3.49	2.53	3.74
	Expt.	4.28 ^b	4.1 ^c	~6.8 ^c	~8.5 ^c	~4.5 ^c	~3.6 ^c	~3.0 ^c	~3.9 ^c
E_v^f (eV)	Pres.	2.14	2.44	2.64	3.16	1.37	1.09	0.86	1.16
	Expt.	2 ^d	2.27 ^e	3.0 ^e	3.1–4.0 ^e	1.79 ^e	1.28 ^e	1.11 ^e	1.70 ^e

^aReference 15.

^bReference 16.

^cReference 17.

^dReference 18.

^eReference 19.

$$E_{defect}^f = E_{Nm,He} - NE_m - E_{He}, \quad (1)$$

where N is the number of metal atoms in the supercell, E_m is the energy per metal atom in a perfect crystal (cohesive energy that is roughly equal to its chemical potential at 0 K), and E_{He} is the energy of an isolated He atom.⁸

III. RESULTS

A single He defect consists of a substitutional or interstitial He atom. In both bcc and fcc structures all the substitutional sites are equivalent, while there are two possibly interstitial sites, i.e., tetrahedral and octahedral positions. These interstitial sites are illustrated in Fig. 1: (a) and (b) for bcc structures and (c) and (d) for fcc structures, respectively. A

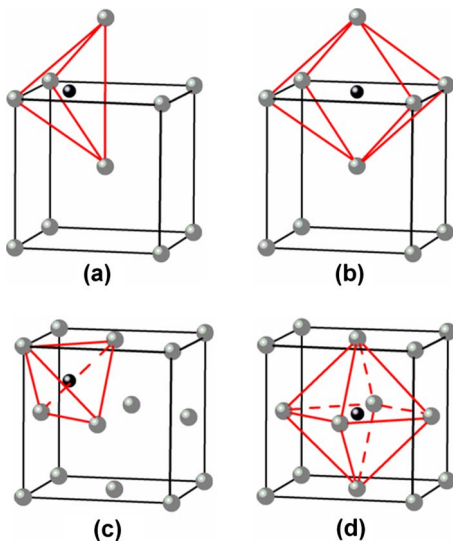


FIG. 1. (Color online) Possible interstitial sites in a bcc structure, (a) tetrahedral and (b) octahedral, and in a fcc structure, (c) tetrahedral and (d) octahedral.

substitutional defect has 8 nearest neighbors at $0.866a_0$ in a bcc structure, while it has 12 nearest neighbors at $0.707a_0$ in a fcc structure. The tetrahedral interstitial has four nearest neighbors at $0.559a_0$ in a bcc structure and four nearest neighbors at $0.433a_0$ in a fcc structure. The octahedral interstitial has six nearest neighbors, with two of them located at $0.5a_0$ and four of them at $0.707a_0$ in a bcc structure, while it has six nearest neighbors at $0.5a_0$ in a fcc structure. It is clear that for both bcc and fcc structures the substitutional site has the largest free volume, followed by the octahedral site, but the tetrahedral site has the smallest one. Since He has a closed-shell electronic structure and bonding interaction is small, He is expected to occupy defect sites in the order of largest free volume, namely, substitutional (sub), octahedral (octa), and tetrahedral (tetra) in both bcc and fcc structures.

In the present work, the He formation energies for the substitutional (E_{sub}^f), the octahedral (E_{octa}^f), and the tetrahedral (E_{tetra}^f) positions calculated using these pseudopotentials by first-principles density functional theory are shown in Tables II and IV for bcc and fcc metals, respectively. For Fe, Ni, and Pd, spin polarized calculations are performed, whereas no polarized calculations are carried out for Mo, Cr, W, Ag, and Cu.

A. bcc metals

The calculations in bcc structures reveal that for all the metals considered, the substitutional position is the most stable site. It is noticed that the tetrahedral position for a He interstitial is energetically more favorable than the octahedral site in bcc structures, and the energy differences between these two positions are 0.19, 0.16, 0.15, and 0.22 eV for Fe, Cr, Mo, and W, respectively, in a 128 atom supercell with 27 k points. In order to study the effect of the supercell size on the results, similar calculations in a small supercell containing 54 atoms with 125 k points were performed. It is of interest to find that changing the supercell size from 128 to 54 atoms slightly affects the formation energies of two He

TABLE II. He formation energies for the substitutional (E_{sub}^f), the octahedral (E_{octa}^f) interstitial, and the tetrahedral (E_{tetra}^f) interstitial positions in bcc metals.

Supercell size	k points	bcc metals	E_{sub}^f (eV)	E_{tetra}^f (eV)	E_{octa}^f (eV)
128 atoms	27	Fe	4.34	4.56	4.75
		Cr	4.83	5.22	5.38
		Mo	4.31	5.33	5.48
		W	4.70	6.19	6.41
54 atoms	125	Fe	4.31	4.49	4.68
		Cr	4.98	5.16	5.32
		Mo	4.39	5.15	5.32
		W	4.83	6.19	6.42

interstitials, but it does not alternate their relative stability in all the bcc metals considered, i.e., the tetrahedral position for a He interstitial is still energetically more favorable than the octahedral site. However, it is widely assumed that the relative stability of a He defect in a bcc structure is associated with the available free volumes of the defect sites, generally following the order of substitutional, octahedral, and tetrahedral positions.⁸ Our first-principles calculations strongly differ from these. In bcc Fe, Seletskaja *et al.*⁸ also noticed that the He tetrahedral interstitial is more stable than the He octahedral interstitial and suggested that this unexpected result maybe lies in the magnetic properties of iron. The strong hybridization between Fe d and He p states affects the properties of the He defect in iron and changes the site preference of the He defects predicted from the classical assumptions. However, Fu and Willaime²⁰ claimed that no hybridization occurs between the closed $1s$ shells of He and the iron valence band, and therefore, there is no evidence of a direct magnetic effect on the relative stabilities of He insertion sites.

In order to understand the real origin of the above discrepancies between *ab initio* calculations and the classical assumptions in a bcc Fe, we have calculated the He formation energies at the tetrahedral and octahedral positions with and

 TABLE III. He formation energies at the tetrahedral and octahedral interstitial positions with and without spin polarization in bcc Fe. The calculations were carried out in a 54 atom supercell with 125 k points.

			E_{octa}^f (eV)	E_{tetra}^f (eV)
Fe (bcc)	Magn.	Full relax.	4.68	4.49
		Nonrel. ^a	6.28	5.74
	No magn.	Full relax.	No convergence	
		Nonrel. ^a	5.86	5.71
		Nonrel. ^b	5.31	5.22

^aThe supercell shape and atomic positions of the system are fixed in the unrelaxed calculations.

^bThe supercell shape and atomic positions of the system are relaxed with magnetism, and then no magnetic electronic structures are calculated without further structural optimization.

without spin polarization in bcc Fe. The results are shown in Table III. It can be seen that for bcc Fe including magnetism, the tetrahedral position of a He interstitial is energetically more favorable than the octahedral site with full relaxation of the crystal. However, the formation energies of these two He interstitials without full relaxation, where the supercell and atomic positions of the system are fixed but electronic structure is relaxed, are given in Table III, which provides the initial energies for comparison. In addition, this also provides an initial insight if the tetrahedral interstitial is more stable than the octahedral interstitial and how the full relaxation affects their relative stability. It is of interest to note that the initial formation energy of the tetrahedral interstitial without full relaxation is lower than that of the octahedral interstitial, which indicates that the relative stability of a He defect in a bcc structure does not follow the classical concept on the available free volumes of the defect sites and may be associated with electronic structure of defects. However, the formation energy decreases due to relaxation, and the differences between the He formation energies at these two interstitial positions decrease from 0.54 to 0.19 eV after relaxation. A bcc Fe without magnetism is not stable under normal conditions, and convergence cannot be achieved for the total energy of the system with full relaxation. In order to address the magnetic effect on the relative stability of He interstitials, the supercell and atomic position of the bcc Fe are first relaxed with magnetism, and then, no magnetic electronic structures are calculated without further structural optimization, i.e., both the supercell shape and the atomic positions are fixed. In addition, the initial energies, as noted by (a), are provided in Table III only for the purpose of comparison, as described above. It is noted that the He formation

 TABLE IV. Formation energies for He atoms in the substitutional (E_{sub}^f), the octahedral (E_{octa}^f), and the tetrahedral (E_{tetra}^f) positions in fcc metals. The calculations were done in a 108 atom supercell with 27 k points.

fcc	Ni	Cu	Ag	Pd
E_{octa}^f (eV)	4.65	3.82	2.68	3.58
E_{tetra}^f (eV)	4.50	3.80	2.79	3.70
E_{sub}^f (eV)	3.23	2.58	1.60	2.24

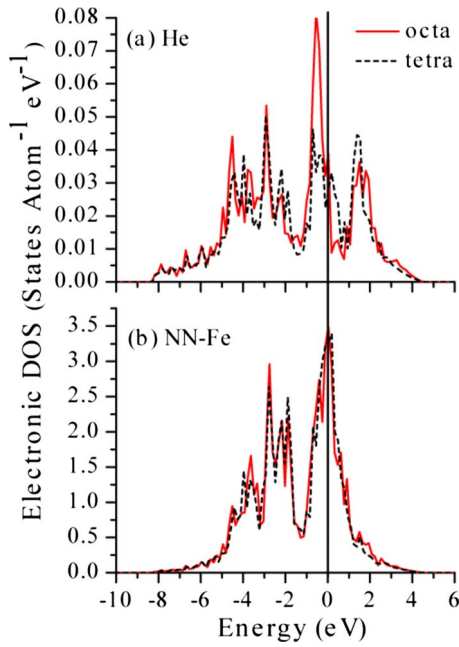


FIG. 2. (Color online) Total DOS of (a) an interstitial He atom at the tetrahedral or octahedral positions and (b) its NN-Fe atoms. The solid and dashed lines represent the total DOS of He interstitials and Fe atoms at tetrahedral and octahedral positions, respectively.

energy at the tetrahedral position is also lower than that at the octahedral position without considering the magnetic properties of Fe, and the difference between the He formation energies at the tetrahedral and octahedral positions is

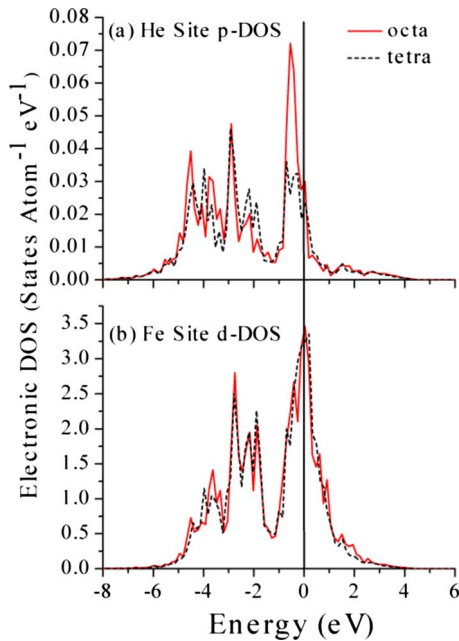


FIG. 3. (Color online) Local DOS of a He interstitial at tetrahedral or octahedral position and its NN-Fe. The solid and dashed lines represent the p -projected DOS of He and d -projected DOS of Fe for the He interstitials at tetrahedral and octahedral positions, respectively.

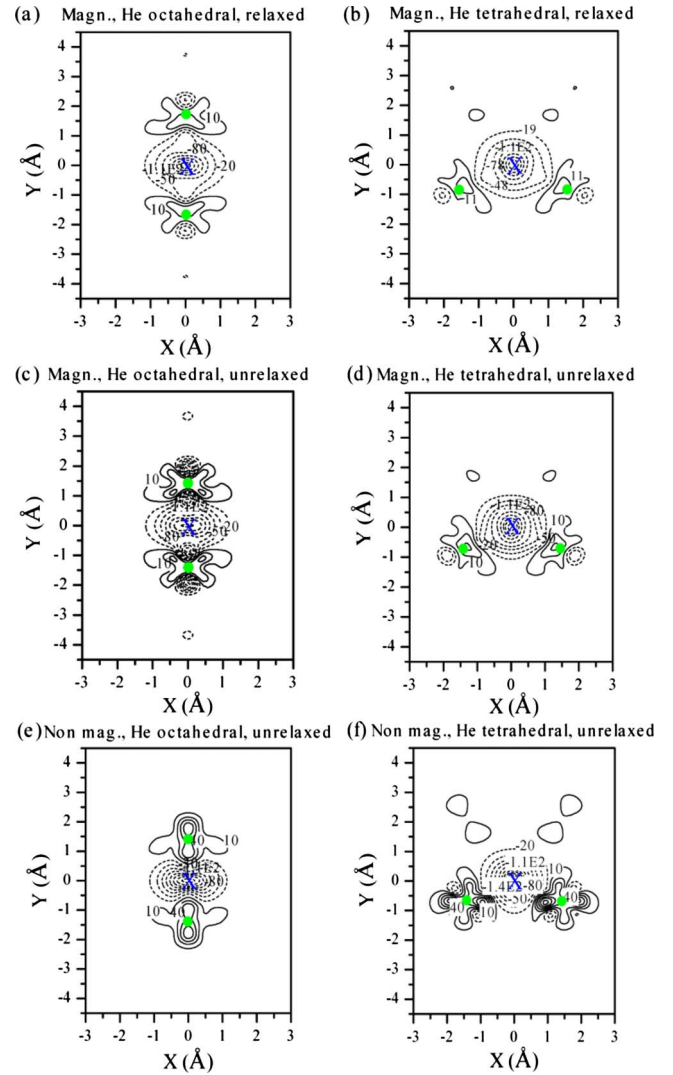


FIG. 4. (Color online) Change in the charge density of Fe due to a He interstitial, where the structures are relaxed with magnetism in (a) and (b), while the structures are not relaxed with magnetism in (c) and (d). Nonmagnetic electronic structures are calculated without any further structural optimization in (e) and (f). The lines represent contours of equivalent charge density ($\times 10^3$) with the same separation of $0.03e/\text{\AA}^3$, whereas the solid lines indicate an increase in charge density and dashed lines represent charge depletion. The cross indicates the position of He and filled gray (green online) circles specify the positions of its nearest-neighbor Fe atoms.

0.15 eV, which is almost the same as that of the calculations with magnetism (0.19 eV). When the supercell shape and the atomic positions of the structures are first relaxed with magnetism and then followed by electronic structure relaxation without magnetism and further structural optimization, the relative energy differences between these two configurations are decreased to 0.09 eV, as shown in Table III. However, these calculations clearly demonstrate that the tetrahedral position is energetically more stable than the octahedral position for a He interstitial, and their relative stability is independent of the magnetic properties.

The reason for the relative stability of the He tetrahedral to octahedral interstitial can be easily understood in terms of

TABLE V. Magnetic moments μ of He atom defects and their neighboring Ni atoms at the separation distances r . The calculations were done in a 108 atom supercell with 27 k points.

	He	First Ni		Second Ni	
	μ (μ_B)	r (\AA)	μ (μ_B)	r (\AA)	μ (μ_B)
Tetra, unrelaxed	0.002	1.524	0.302	2.918	0.607
Tetra, relaxed	0.011	1.767	0.487	2.939	0.606
Octa, unrelaxed	0.018	1.760	0.506	3.048	0.616
Octa, relaxed	0.01	1.932	0.563	3.061	0.615
Sub, unrelaxed	0.000	2.488	0.613	3.519	0.602
Sub, relaxed	0.000	2.506	0.618	3.503	0.604

the total electronic DOSs of the He atom and its nearest-neighbor Fe (NN-Fe). Figure 2 shows the total DOS of a He interstitial at tetrahedral or octahedral position and its NN-Fe atoms when no magnetic electronic structures are considered and without further structural optimization. The position of the Fermi level relative to the peaks in the density of states determines the occupation of the states and the nature of bonding.²¹ It can be seen from Fig. 2 that the interaction of tetrahedral He interstitial with its neighbor Fe atoms leads to a lower DOS of He atoms at the Fermi level than that of the octahedral interstitial, which indicates the stronger bonding at the tetrahedral interstitial site. However, the total DOS of NN-Fe atoms is almost the same for the two He interstitial configurations. Figure 3 presents the p -projected DOS of these two He interstitials and the d -projected DOS of the NN-Fe atoms under the same calculation conditions. The similarity in the shapes of the Fe d and He p DOSs reflects that strong hybridization occurs between the Fe d and He p states without magnetism, in contrast to the previous investigation, where magnetic properties give rise to the strong hybridization between the Fe d and He p states, which leads to the tetrahedral He interstitial being more stable in bcc Fe.

Figure 4 shows the changes in the charge densities produced by the He octahedral and tetrahedral defects in the relaxed and unrelaxed structures with magnetism, as well as in unrelaxed structures without magnetism. From Fig. 4, it is

 TABLE VI. Formation energies of He defects at the tetrahedral and octahedral positions with and without spin polarization in fcc Ni. The calculations were done in a 108 atom supercell with 27 k points.

			E_{octa}^f (eV)	E_{tetra}^f (eV)
Ni (fcc)	Magn.	Full relax.	4.65	4.50
		No magn.	4.61	4.37
		Nonrel. ^a	5.43	5.85
		Nonrel. ^b	4.59	4.36

^aThe supercell shape and atomic positions of the system are fixed in the unrelaxed calculations.

^bThe supercell shape and atomic positions of the system are relaxed with magnetism, and then no magnetic electronic structures are calculated without further structural optimization.

of interest to find that the He interstitial and its nearest-neighbor Fe atoms are all polarized due to the strong interactions between them with and without spin polarization. From Figs. 4(a)–4(d), it is clear that when the structures are not relaxed with magnetism, the polarization is very strong, which results in the high formation energy of the He interstitial, as shown in Table III. After atomic relaxation the formation energy decreases significantly due to the decrease in polarization, and the change in the charge densities produced by the octahedral He interstitial is more significant than that by the tetrahedral He, but the order of site preference for the He interstitials does not change. Furthermore, Figs. 4(c) and 4(e) illustrate that the polarization of Fe due to the octahedral interstitial He decreases without considering magnetism, which leads to the decrease in the formation energy of the octahedral He interstitial. Figures 4(d) and 4(f) clearly show that the polarization of Fe produced by the tetrahedral He interstitial increases without considering magnetism, but the formation energy of the tetrahedral interstitial He atoms remains almost the same. These results suggest that the difference of the formation energy between the octahedral and tetrahedral interstitial He atoms decreases without considering magnetism. However, the decrease is not enough to revise the order of their relative stability, which suggests that the magnetism in bcc Fe slightly affects the formation energy of He interstitials but does not alter their relative stabilities.

B. fcc metals

Table IV shows the formation energies of He atoms in the substitutional, octahedral, and tetrahedral positions in the fcc structure. The substitutional position is also the most stable site for all the fcc metals considered. Furthermore, the tetrahedral He interstitial is energetically more favorable than the octahedral site in fcc Ni, but the octahedral He interstitial is energetically more favorable than the tetrahedral interstitial in fcc Ag and Pd. The formation energies of He interstitials at the tetrahedral and octahedral positions in fcc Cu are nearly the same, with a difference of only 0.03 eV.

In order to identify magnetic effects on the relative stability of He defect sites in Ni, the magnetic moments of the He defects and their neighboring Ni atoms are calculated in a 108 atom supercell, and the corresponding results are pre-

sented in Table V for both relaxed and unrelaxed configurations. The magnetic moment of Ni in a perfect fcc structure is calculated to be $0.603\mu_B$. It can be seen that the He defects change the magnetic moments of their first- and second-nearest-neighbor Ni atoms. The magnetic moment of the first neighbor Ni atoms increases with increasing He-Ni distance. However, the largest change in the magnetic moment of Ni ($-0.185\mu_B$) occurs with He in the tetrahedral position, and relaxation does not restore the full Ni moment. The tetrahedral position is more stable than the octahedral site, which is the same result obtained in bcc Fe, but it is in contrast to the variation in the magnetic moments of the previous study in bcc Fe.⁸ For bcc Fe, the largest change in the magnetic moments of Fe atoms occurs when the He octahedral interstitial is in the unrelaxed structure, where the distance between He and Fe is the largest. The difference between them may be due to their structures. However, the largest change in the magnetic moments of Ni atoms corresponds to the He tetrahedral interstitial in the unrelaxed structure of fcc Ni, where the distance between He and Ni is also the largest. These results further demonstrate that the change in the magnetic moments of host atoms are correlated with the distances between the He atom and the host atoms but not directly related to the relative stability of He interstitial sites.

Similar to the analysis in Fe, the formation energies of He interstitials at the tetrahedral and octahedral positions with and without spin polarization are calculated in a fcc Ni, which is shown in Table VI. The calculated results of Ni without magnetism are not the same as those of Fe. The tetrahedral interstitial is energetically more favorable than the octahedral interstitial with full relaxation, which does not

depend on whether the magnetic properties of Ni are considered or not. However, when the structures are not relaxed with magnetism and nonmagnetic electronic structures are considered without further structural optimization, the calculated results show that the He octahedral interstitial is energetically more favorable than the tetrahedral site. If the structures are relaxed with magnetism and then nonmagnetic electronic structures are calculated without further structural optimization, the tetrahedral position becomes the more stable of the two interstitial sites.

IV. CONCLUSIONS

The relative stabilities of He interstitial sites in bcc and fcc metals are calculated using *ab initio* calculations based on density functional theory, and the results show the different behaviors of defects in bcc and fcc metals. For the bcc metals considered, the He tetrahedral interstitial is energetically more favorable than the octahedral site, but for the fcc metals the relative stability of He interstitials varies. It is important to note that including magnetic effects slightly changes the properties of the He defects in both bcc and fcc metals, but it does not directly affect the relative stabilities of He interstitials. The present results demonstrate that the relative stabilities of He interstitials are primarily associated with the bonding properties of He defects and host atoms.

ACKNOWLEDGMENT

The authors (F.G., H.L.H., and R.J.K.) are grateful for support by the U.S. Department of Energy/Office of Fusion Energy Science under Contract No. DE-AC06-76RLO 1830.

*xiaotaozu@yahoo.com

†fei.gao@pnl.gov

¹S. J. Zinkle, *Phys. Plasmas* **12**, 058101 (2005).

²Y. Ishiyama, M. Kodama, N. Yokota, K. Asano, T. Kato, and K. Fukuya, *J. Nucl. Mater.* **239**, 90 (1996).

³R. E. Stoller and G. R. Odette, *J. Nucl. Mater.* **154**, 286 (1988).

⁴M. B. Lewis and K. Farrell, *Nucl. Instrum. Methods Phys. Res. B* **16**, 163 (1986).

⁵R. Vassen, H. Trinkaus, and P. Jung, *Phys. Rev. B* **44**, 4206 (1991).

⁶Y. Katoh, M. Ando, and A. Kohyama, *J. Nucl. Mater.* **323**, 251 (2003).

⁷B. B. Nielsen and A. van Veen, *J. Phys. F: Met. Phys.* **15**, 2409 (1985).

⁸T. Seletskaiya, Y. Osetsky, R. E. Stoller, and G. M. Stocks, *Phys. Rev. Lett.* **94**, 046403 (2005).

⁹G. Kresse and J. Hafner, *Phys. Rev. B* **47**, 558 (1993).

¹⁰G. Kresse and J. Furthmüller, *Phys. Rev. B* **54**, 11169 (1996).

¹¹G. Kresse and J. Furthmüller, *Comput. Mater. Sci.* **6**, 15 (1996).

¹²G. Kresse and D. Joubert, *Phys. Rev. B* **59**, 1758 (1999).

¹³P. E. Blöchl, *Phys. Rev. B* **50**, 17953 (1994).

¹⁴J. P. Perdew, J. A. Chevary, S. H. Vosko, K. A. Jackson, M. R. Pederson, D. J. Singh, and C. Fiolhais, *Phys. Rev. B* **46**, 6671 (1992); **48**, 4978(E) (1993).

¹⁵www.webelements.com

¹⁶C. Kittel, *Introduction to Solid State Physics*, 7th ed. (Wiley, New York, 1996).

¹⁷C. Kittel, *Introduction to Solid State Physics*, 4th ed. (Wiley, New York, 1971).

¹⁸L. De Schepper, D. Segers, L. Dorikens-Vanpraet, M. Dorikens, G. Knuyt, L. M. Stals, and P. Moser, *Phys. Rev. B* **27**, 5257 (1983).

¹⁹K. Maier, M. Peo, B. Saile, H. E. Schaefer, and A. Seeger, *Philos. Mag. A* **40**, 701 (1979).

²⁰C.-C. Fu and F. Willaime, *Phys. Rev. B* **72**, 064117 (2005).

²¹R. Pentcheva and M. Scheffler, *Phys. Rev. B* **65**, 155418 (2002).